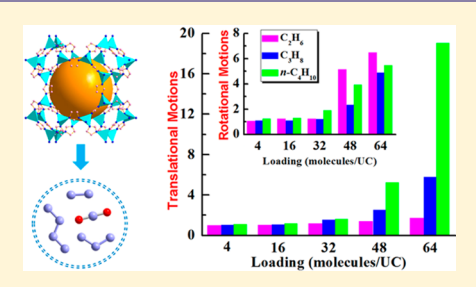


# Molecular-Level Understanding of Translational and Rotational Motions of $C_2H_6$ , $C_3H_8$ , and $n-C_4H_{10}$ and Their Binary Mixtures with CO<sub>2</sub> in ZIF-10

Li Li,<sup>†</sup> Guobing Zhou,<sup>‡</sup> Zhen Yang,\*,<sup>†</sup> Fang Fang,<sup>†</sup> Qi Qiao,<sup>‡</sup> Na Hu,<sup>†</sup> Liangliang Huang,\*,<sup>‡</sup> and Xiangshu Chen\*, T

Supporting Information

ABSTRACT: Molecular dynamics simulations have been employed to investigate the translational and rotational motions of C<sub>2</sub>H<sub>6</sub>, C<sub>3</sub>H<sub>8</sub>, and n-C<sub>4</sub>H<sub>10</sub> and their binary mixtures with CO<sub>2</sub> in ZIF-10 at a molecular level. Our simulation results reveal that the translational motions of pure alkanes in ZIF-10 decrease monotonically with the increasing loading partly due to the competition between the enhanced alkane-alkane and the weakened alkane-ZIF interactions. Also, the increasing collision frequency with loading can hinder their translational motions considerably. However, their rotational motions are found to be initially accelerated and then decelerated gradually beyond a critical loading for all studied alkanes. The initial acceleration of their rotational motions is due to more alkane



molecules not being adsorbed at the internal surfaces but into the free central regions of cages in ZIF-10 as the loading increases. Furthermore, a loading higher than the corresponding critical value can result in a considerable decrease in free spaces in whole ZIF-10 so that more restrictions hinder their rotational motions. On the other hand, the presence of CO<sub>2</sub> molecules promotes both the translational and rotational motions of alkanes in ZIF-10 for all studied alkane/CO<sub>2</sub> mixtures, most significantly for n-C<sub>4</sub>H<sub>10</sub>/CO<sub>2</sub>. Besides the small size of CO<sub>2</sub> molecules, the strong hydrogen bonds with the imidazolate rings can cause CO<sub>2</sub> molecules to preferentially occupy the adsorption sites of ZIF-10 compared to alkanes, leading to the weakened interactions between alkanes and ZIF-10. More importantly, such competitive adsorption with CO<sub>2</sub> in the mixture cases also results in a noticeable decrease in the collision frequency for alkanes in ZIF-10, which is in turn favorable to the enhanced translational and rotational motions of alkanes in ZIF-10. In addition, the confinement of ZIF-10 is also found to significantly promote the acceleration effect of CO<sub>2</sub> molecules on the translational and rotational motions of alkanes.

#### 1. INTRODUCTION

Light alkanes are commonly regarded as the most important chemical raw materials for commodity production in the fuels and chemical industry. 1-3 Actually, light alkanes often contain impurities in production processes, such as N2, CO2, H2S, and H<sub>2</sub>O.<sup>4</sup> In particular, CO<sub>2</sub> is one of the most widespread impurities and can often be corrosive to gas pipelines.5 Meanwhile,  $C_2H_6$  can form a maximum-pressure azeotrope with  $CO_2$ which will hinder CO2 removal via distillation or other effective natural gas treatments.<sup>6</sup> Therefore, efficiently removing CO<sub>2</sub> from light alkanes is still a great challenge in fully utilize light alkanes, such as natural gas purification, biogas and landfill gas upgrading, 8,9 and enhanced oil recovery. 10 In past decades, adsorption- and membrane-based separations by nanoporous materials have been widely accepted as promising cost-efficient techniques. <sup>11–19</sup> The separation performance is mainly determined by the differences in both selective adsorption and diffusion properties between different components in nanoporous materials. 19-25 Therefore, it is critical to gain a molecular-level understanding of the relevant adsorption

and diffusion mechanism of gas mixtures in nanoporous materials.

Until now, many experimental and simulation studies have focused on the adsorption and diffusion behavior of light alkanes and their mixtures with CO2 in various porous materials. 12,13,25-35 Experimentally, Patankar et al. 32 investigated the properties of C<sub>2</sub>H<sub>6</sub> and the C<sub>2</sub>H<sub>6</sub>/CO<sub>2</sub> mixture confined in mesoporous controlled pore glass (CPG) silica, showing that CO2 has a stronger affinity for the CPG silica than for C<sub>2</sub>H<sub>6</sub>, which should be responsible for the increasing mobility of C<sub>2</sub>H<sub>6</sub> due to the displacement of C<sub>2</sub>H<sub>6</sub> molecules from adsorption sites by CO<sub>2</sub>. On the contrary, Luo et al.<sup>33</sup> found that C<sub>3</sub>H<sub>8</sub> molecules have an adsorption preference in small-pore zeolites (i.e., zeolite T, SSZ-13, and SAPO-34) compared to CO2, where C3H8 can displace some CO2 from the adsorption site and hinder the permeation of CO2. On the

Received: July 27, 2018 Accepted: December 31, 2018 Published: January 14, 2019

<sup>&</sup>lt;sup>†</sup>Institute of Advanced Materials (IAM), State-Province Joint Engineering Laboratory of Zeolite Membrane Materials, College of Chemistry and Chemical Engineering, Jiangxi Normal University, Nanchang 330022, People's Republic of China

<sup>&</sup>lt;sup>‡</sup>School of Chemical, Biological and Materials Engineering, University of Oklahoma, Norman, Oklahoma 73019, United States

other hand, Borah et al.<sup>34</sup> used molecular dynamics (MD) simulations to investigate the diffusion properties of pure  $CH_4$ ,  $C_2H_6$ ,  $C_3H_8$ , and  $C_4H_{10}$  as well as their binary mixtures with  $CH_4$  in six MOFs with different topologies and pore sizes. The diffusion coefficients of the alkanes follow the order  $CH_4 > C_2H_6 > C_3H_8 > C_4H_{10}$  in the study of MOFs and decrease gradually with increasing chain length. Le and Striolo<sup>35</sup> employed MD simulations to investigate the relationship between the structure and dynamics of  $CO_2/C_4H_{10}$  mixtures in fully protonated silica slit nanopores, where the presence of  $CO_2$  molecules can enhance the self-diffusion motions of n- $C_4H_{10}$  because the preferential  $CO_2$  adsorption to the pore walls can reduce the diffusion activation energy of n- $C_4H_{10}$ .

Recently, zeolitic imidazolate frameworks (ZIFs), as a new subfamily of metal-organic frameworks (MOFs), have attracted considerable attention in practical gas storage and separation due to their exceptional chemical and thermal stabilities in both aqueous and organic media compared to other MOFs. 36-45 For example, Gücüyener et al. 43 showed that ZIF-7 exhibits excellent selective adsorption of C<sub>2</sub>H<sub>6</sub> over C<sub>2</sub>H<sub>4</sub> in their mixture through the gate-opening effect. Keskin<sup>44</sup> employed grand canonical Monte Carlo (GCMC) and MD simulations to study the adsorption and diffusion properties of CH<sub>4</sub>/H<sub>2</sub>, CO<sub>2</sub>/CH<sub>4</sub>, and CO<sub>2</sub>/H<sub>2</sub> mixtures in ZIF-3 and ZIF-10, respectively, showing that both ZIF-3 and ZIF-10 exhibit considerably higher adsorption selectivity compared to many common MOFs. Sholl and co-workers 45 have calculated the self- and transport diffusion coefficients of CH<sub>4</sub>, C<sub>2</sub>H<sub>6</sub>, C<sub>3</sub>H<sub>8</sub>, n-C<sub>4</sub>H<sub>10</sub>, and other light hydrocarbons in fully flexible ZIF-8 by dynamically corrected transition-state theory. Most of their self-diffusion coefficients show an increase with loading, which is attributed to the larger decrease in the diffusion free energy barrier compared to the reduction of the transmission coefficient due to the increased number of gas-gas collisions. 45 Despite great effort, however, the diffusion mechanism of light alkanes and their mixtures with CO2 in ZIFs is far from a complete understanding.

Besides the diffusion motions, which are essentially the translational motions, the rotational motions of light alkanes in ZIFs should also play an important role in the relevant separation processes as the chain length of alkanes increases, which is more unclear at present. Actually, the rotational motions of molecules confined in porous media have been confirmed to be closely related to their translational motions. 46-For example, Reimer and co-workers<sup>46</sup> combined NMR and MD simulation to explore different xylene isomers in MOF-5. Paraxylene was experimentally observed to have the fastest translational motions at all temperatures but the slowest rotational motions. Their MD simulations confirmed that the construction of rotational freedom in an isotropically confined geometry leads to a faster translational motion of the most rodlike molecules (i.e., paraxylene). However, neither metaxylene nor orthoxylene experienced comparable restrictions for in-plane rotations when adsorbed in MOF-5. Maurin and co-workers<sup>47</sup> explored the loading-dependent diffusion mechanism for light alkanes including C<sub>2</sub>H<sub>6</sub>, C<sub>3</sub>H<sub>8</sub>, and n-C<sub>4</sub>H<sub>10</sub> in the flexible MOF MIL-53(Cr) by combining quasi-elastic neutron scattering measurements (QENS) and MD simulations. According to their results, the diffusion rates of C2H6 and C<sub>3</sub>H<sub>8</sub> molecules decrease monotonically with the increasing loading, while that of n-C<sub>4</sub>H<sub>10</sub> follows an unusual increase at a higher concentration due to the reopening of a flexible MOF. Moreover, they also found that the global translational

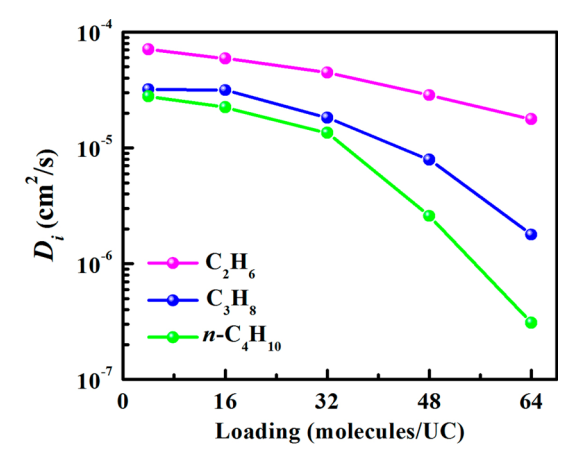


**Figure 1.** Variation of the self-diffusion coefficients  $D_i$  with loading for pure alkanes of  $C_2H_6$ ,  $C_3H_8$ , and n- $C_4H_{10}$  molecules in ZIF-10. The relevant values and standard deviations are listed in Table S4 of the Supporting Information.

motion is associated with rotational dynamics, where  $n\text{-}C_4H_{10}$  follows uniaxial rotational motions within the pore while  $C_2H_6$  displays random rotational reorientation. Kolokolov et al. employed experimental (QENS and NMR) and computational (MD) tools to investigate the diffusion behavior of benzene in MIL-53(Cr). They found that benzene uses a 1D-jump translational diffusion mechanism, which is combined with a fast uniaxial rotational motion around the  $C_6$  axis. In this way, benzene can be thought of as a rotating disc that diffuses rapidly through the central part of the MIL-53 channel by short jumps between neighboring low-energy basins.

To this end, a series of MD simulations have been carried out to systematically investigate at a molecular level the translational and rotational motions of light alkanes (including  $C_2H_6$ ,  $C_3H_8$ , and  $n\text{-}C_4H_{10}$ ) and their equimolar mixtures with  $CO_2$  in ZIF-10. Herein, we mainly focus on the loading-dependent translational and rotational motions of light alkanes confined in ZIF-10 and how the presence of  $CO_2$  molecules affects these dynamic properties. This article is organized as follows. In section 2, we present the details of MD simulations. Then, the simulation results for the pure and binary mixture components will be discussed and analyzed in section 3. Finally, we offer a few general conclusions and remarks in section 4.

#### 2. SIMULATION DETAILS

In this work, the crystal structure of ZIF-10 for MD simulations was constructed from the experimental X-ray diffraction data of the Cambridge Structural Database (CSD).<sup>49</sup> In the framework of ZIF-10, each Zn atom is tetrahedrally bridged by four imidazolate linkers, resulting in a merlinoite (MER) zeolite-type cage of ~12.1 Å in diameter connected by large windows of 8.2 Å in diameter, and there are two MER cages in each unit cell (UC). The recent force field proposed by Zheng et al.<sup>50</sup> was employed for ZIF-10. Although the flexible force fields are more reasonable than the rigid ones in general, it should be noted that the ZIF-10 structure was rigid during the following MD simulations as a result of the limitations of the available force field. 51,52 Actually, when the window sizes of nanoporous materials are comparable to the kinetic diameter of gas molecules, the free-energy barrier from the windows will dominate the diffusion of gas molecules, and the corresponding diffusion coefficients often increase with loading. 20,45 In this

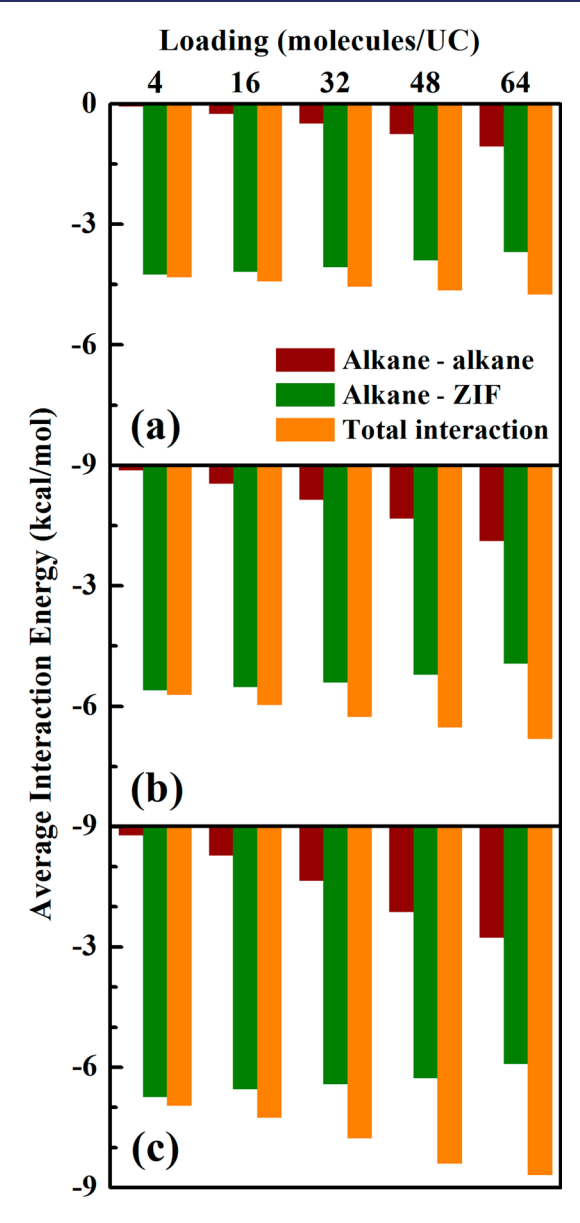


**Figure 2.** Average interaction energies of alkane—alkane, alkane—ZIF, and the total interaction energy for pure (a)  $C_2H_6$ , (b)  $C_3H_8$ , and (c) n- $C_4H_{10}$  molecules in ZIF-10 at different loadings. All standard deviations here are less than  $\pm 0.02$  kcal/mol. The error bars are smaller than the symbol size, so they are not shown.

case, the flexible force fields used for ZIFs are necessary, but when the window sizes are larger than the kinetic diameter of a gas molecule, the diffusion of the gas molecule is determined by the steric hindrance between diffusing molecules and the corresponding diffusion coefficients decrease with loading.  $^{21,22,34,53}$  In this work, the window openings of ZIF-10 (8.2 Å) are much larger than the kinetic diameters of  $CO_2$  (3.3 Å),  $^{39}$   $C_2H_6$  (4.0 Å),  $^{41}$   $C_3H_8$  (4.3 Å),  $^{54}$  and  $n\text{-}C_4H_{10}$  (4.3 Å) molecules. In the following section, the diffusion coefficients are found to decrease with loading, suggesting that the flexibility of ZIF-10 may have a negligible influence on the confined properties of the studied gas molecules. Meanwhile, the TraPPE united atom model was used for the  $C_2H_6$ ,  $C_3H_8$ , and  $n\text{-}C_4H_{10}$  molecules,  $^{55}$  while a three-site model was used for  $CO_2$  and partial point charges are centered at each site to present the quadrupole moment.  $^{56}$  Herein, the nonbonded interactions were described by the combination of electrostatic

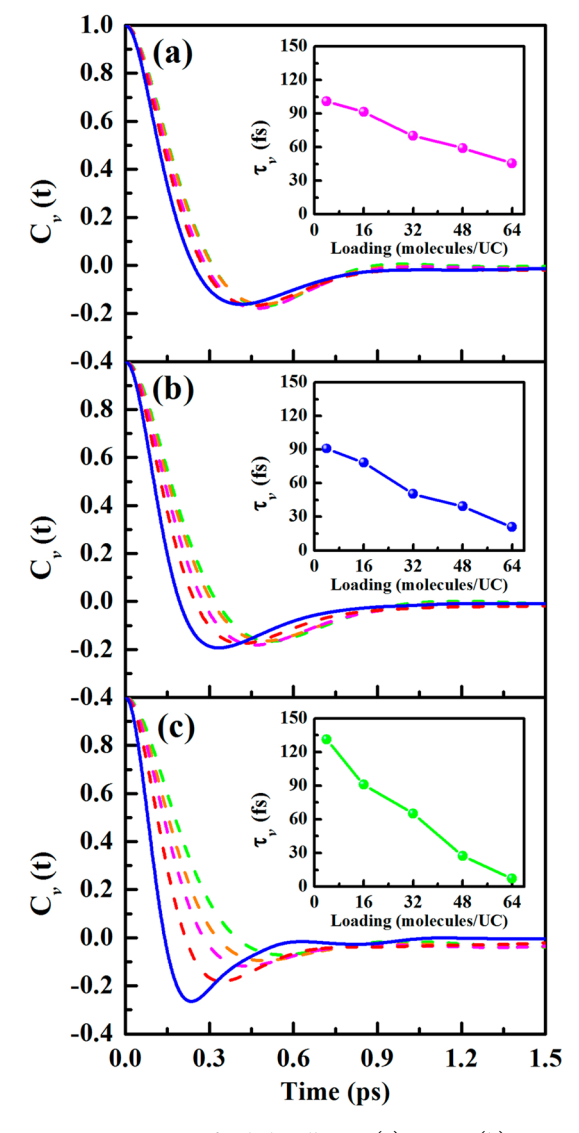


**Figure 3.** VACF curves for light alkanes (a)  $C_2H_6$ , (b)  $C_3H_8$ , and (c)  $n\text{-}C_4H_{10}$  molecules in ZIF-10 at different loadings. Lines colored green, orange, magenta, red, and blue correspond to loadings from 4 to 64 molecules/UC in turn. The inset shows the corresponding relaxation times. All standard deviations here are less than  $\pm 1.5$  fs. The error bars are smaller than the symbol size, so they are not shown.

and Lennard-Jones (L-J) interactions. All L-J parameters and partial atomic charges used in this work were summarized and listed in Tables S1 and S2 in the Supporting Information. Then, the Lorenz-Berthelot mixing rules were employed to calculate the crossing L-J interaction parameters.

A series of NVT MD simulations were conducted to explore the diffusion behavior for the pure components of  $C_2H_6$ ,  $C_3H_8$ ,  $n\text{-}C_4H_{10}$ , and their equimolar mixtures with  $CO_2$  in ZIF-10 with a variety of loadings (i.e., 4, 16, 32, 48, and 64 gas molecules were initially arranged into a single UC by using the configuration-biased insertion technique<sup>57</sup>). Then, each initial configuration was obtained by making a supercell from the corresponding unit cell (ZIF-10 with gas molecules) in three directions. The compositions of alkane/ $CO_2$  mixtures in bulk phases corresponding to the counterparts confined in ZIF-10 were calculated via grand canonical Monte Carlo (GCMC) calculations and have been summarized in Table S3 in the Supporting Information. It is worth noting that our simulation setup is to have a predefined loading in ZIF-10 and that the

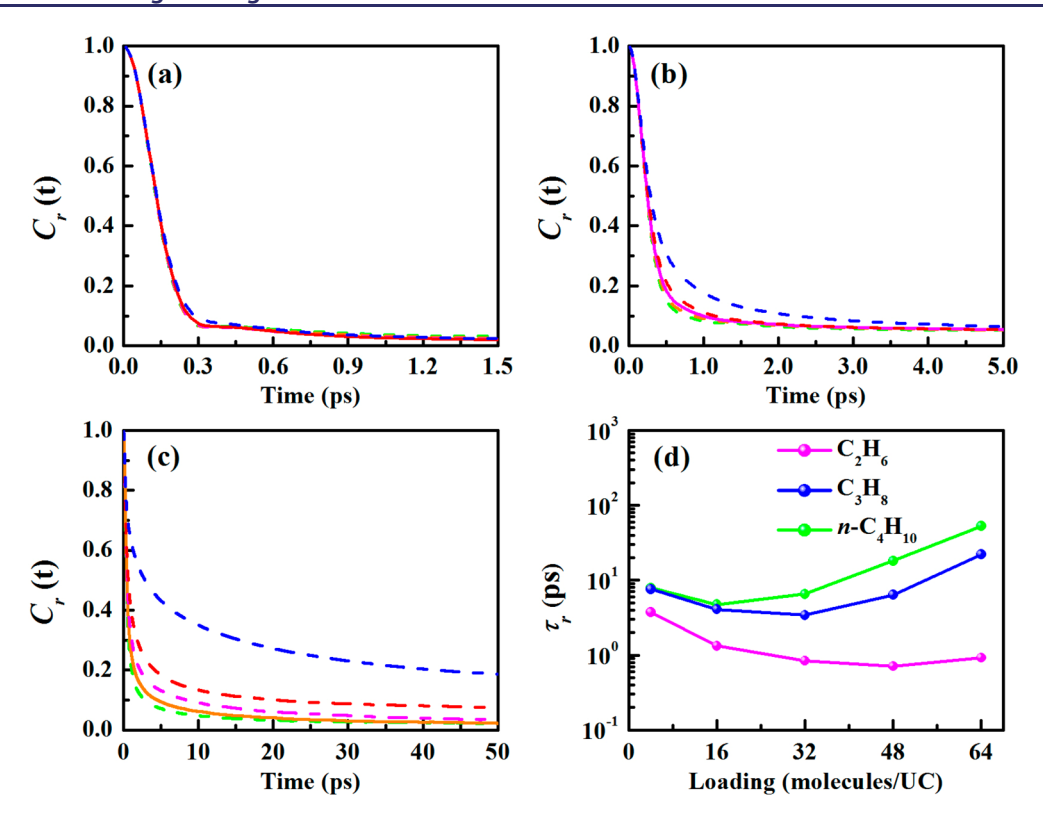
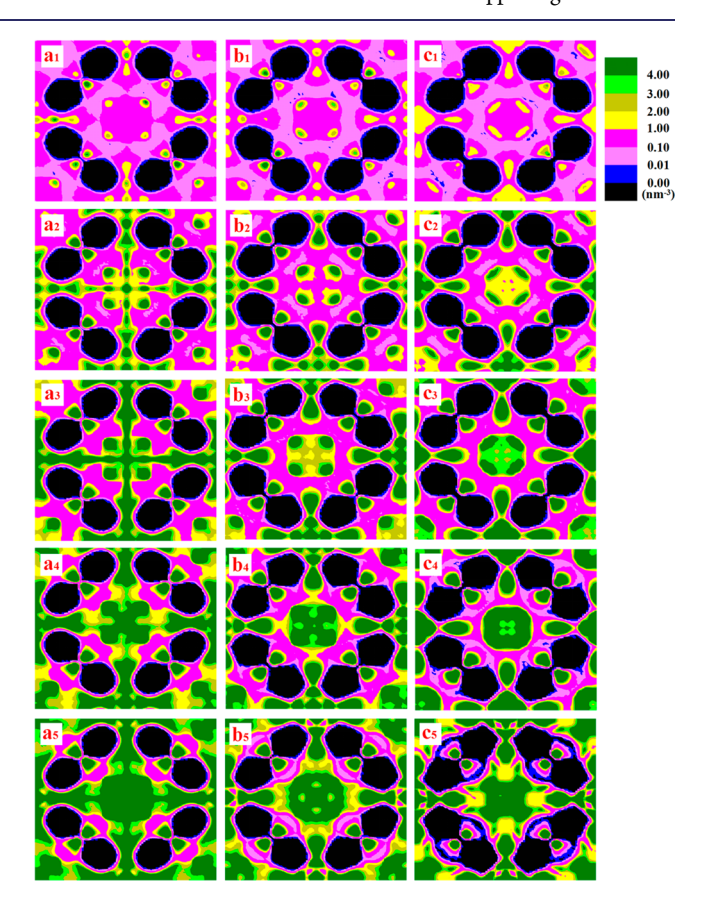


Figure 4. Rotational TCFs of (a)  $C_2H_6$ , (b)  $C_3H_8$ , and (c) n- $C_4H_{10}$  molecules in ZIF-10 at different loadings as well as (d) the corresponding rotational relaxation times. Green, orange, magenta, red, and blue lines correspond to the loadings from 4 to 64 molecules/UC in turn. Here the rotational TCFs are constructed using the second-order Legendre polynomial. The relevant values and standard deviations are listed in Table S6 of the Supporting Information.

corresponding bulk-phase pressure could be as high as a few hundred atmospheres, which is unlikely to represent a real separation application. As shown in the previous work, 58,59 the size of the simulation box has a considerable influence on the diffusion coefficients due to the particle numbers and the calculation of long-range electrostatic interactions. To accommodate enough gas molecules, 60 two larger simulation boxes were composed of  $4 \times 4 \times 4$  and  $3 \times 3 \times 3$  UCs for the low loadings of 4 and 16 molecules/UC, respectively, which should be able to better eliminate the statistical uncertainties of diffusion coefficients. It should be noted that there are 34 816 atoms in the framework of ZIF-10 when the simulation box is  $4 \times 4 \times 4$  UCs. Meanwhile, a smaller simulation box of  $2 \times 2$ × 2 UCs was used for other higher loadings. Therefore, the dimensions of these simulation boxes with the periodic boundary conditions in three directions are  $54.12 \times 54.12 \times 38.81 \text{ Å}^3$  for  $2 \times 2 \times 2$  UCs,  $81.18 \times 81.18 \times 58.22$  Å<sup>3</sup> for  $3 \times 3 \times 3$  UCs, and  $108.24 \times 108.24 \times 77.62 \text{ Å}^3$  for  $4 \times 4 \times 4 \text{ UCs}$ .

For each loading, at least three MD simulations with independent initial configurations were carried out in the canonical (NVT) ensemble, where the temperature was fixed at 303.0 K and controlled by the Nosé–Hoover algorithm. Newton's equation of motion was integrated by the velocity-Verlet algorithm with a time step of 1.0 fs. A cutoff of 10 Å was applied for the nonbonded interactions, and the long-range electrostatic interactions were treated by the particle–particle particle-mesh (PPPM) method. In each MD simulation, we ran the first 20 ns for equilibration, and then the next simulation from 30 to 100 ns was performed for trajectory analyses, with the trajectories stored every 100 fs. Subsequently, an additional NVT MD simulation of 500 ps (following the corresponding final configuration attained from the above calculation)



**Figure 5.** Two-dimensional density distribution in the x-y plane of pure (a)  $C_2H_6$ , (b)  $C_3H_8$ , and (c) n- $C_4H_{10}$  molecules in ZIF-10. Loadings from 4 to 64 molecules/UC corresponding to  $a_1-a_5$ ,  $b_1-b_5$ , and  $c_1-c_5$ .

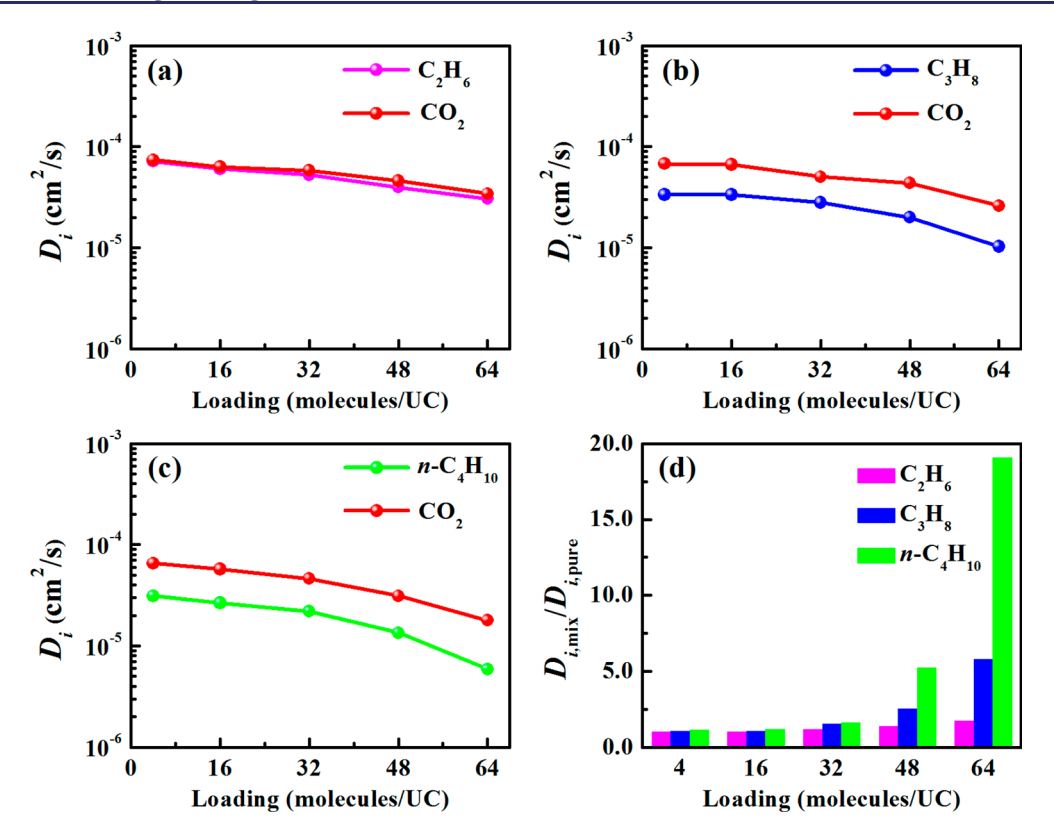


Figure 6. Variation of self-diffusion coefficients  $D_i$  with loading for binary (a)  $C_2H_6/CO_2$ , (b)  $C_3H_8/CO_2$ , and (c) n- $C_4H_{10}/CO_2$  mixtures as well as (d) the  $D_{i,mix}/D_{i,pure}$  ratio. The relevant values and standard deviations are listed in Table S5 of the Supporting Information.

was performed for each simulation system, but their trajectories and velocities were saved every time step (i.e., 1 fs) to better calculate the velocity autocorrelation functions. In this work, all NVT MD simulations were performed by using the large-scale atomic/molecular massively parallel simulator (Lammps) software package. It should be noted that all standard deviations reported in this work are the population standard deviation, calculated by  $\sigma = \sqrt{\frac{1}{N} \sum_{i=1}^{N} \left(x_i - \overline{x}\right)^2}$ , where N is the block number of each system. After equilibrium, the trajectory of a production run was divided into 3 to 10 blocks to guarantee that each block covers 10 ns of data.

# 3. RESULTS AND DISCUSSION

**3.1. Pure Alkanes in ZIF-10.** First, the translational motions of pure light alkanes in ZIF-10 can be well specified with the self-diffusivity of the center of mass (COM), and the corresponding self-diffusion coefficients  $D_i$  can be calculated via the relevant mean square displacement (MSD) based on Einstein's formulation  $^{63,64}$ 

$$D_{i} = \lim_{t \to \infty} \frac{\langle [\mathbf{r}_{i}(t) - \mathbf{r}_{i}(0)]^{2} \rangle}{6t}$$
 (1)

where  $\langle [\mathbf{r}_i(t) - \mathbf{r}_i(0)]^2 \rangle$  is the MSD of the *i*th kind of gas molecule at a certain time *t*. The angular bracket means that the ensemble average is taken over all tagged gas molecules at different reference initial times. The calculated MSD curves of  $C_2H_6$ ,  $C_3H_8$ , and n- $C_4H_{10}$  molecules are shown in Figure S1 of the Supporting Information, where  $C_3H_8$  and n- $C_4H_{10}$  molecules in ZIF-10 are found to have obvious subdiffusive behavior at the highest loading of 64 molecules/UC. Then, Figure 1 presents the calculated self-diffusion coefficients  $D_i$  of

pure alkanes in ZIF-10 as a function of the loading. We can observe that all values of  $D_i$  for different pure alkanes in ZIF-10 decrease monotonically with increasing loading and their diffusion rates always follow the order  $\rm C_2H_6 > \rm C_3H_8 > \it n-\rm C_4H_{10}$  (3.10 ×  $10^{-7}~\rm cm^2~s^{-1}$ ) is far less than that of  $\rm C_2H_6$  (1.77 ×  $10^{-5}~\rm cm^2~s^{-1}$ ) by around 60 times at the highest loading of 64 molecules/UC. A larger  $D_i$  difference between  $\rm C_2H_6$  (2.57 ×  $10^{-8}~\rm cm^2~s^{-1}$ ) and  $\it n-\rm C_4H_{10}$  (8.85 ×  $10^{-11}~\rm cm^2~s^{-1}$ ) molecules can be observed in ZIF-8<sup>44</sup> due to the smaller window of ZIF-8 ( $\it d_w = 3.8~\rm Å$ ) compared to that of ZIF-10 ( $\it d_w = 8.2~\rm Å$ ). Meanwhile, the self-diffusion coefficients  $D_i$  for pure alkanes in ZIF-10 are found to have a slight decrease at low loadings, followed by a rapid decrease as the loading increases, especially for the  $\rm C_3H_8$  and  $\it n-\rm C_4H_{10}$  molecules.

Generally, the loading-dependent diffusion behavior of gas molecules in ZIFs is determined by the competition between both the gas-gas and gas-ZIF interactions. Figure 2 shows the average alkane-alkane and alkane-ZIF interaction energies for  $C_2H_6$ ,  $C_3H_8$ , and n- $C_4H_{10}$  molecules in ZIF-10 over the studied loading range, as well as the corresponding total interaction energies. All average interaction energies are found to be negative, and their absolute values correspond to the magnitude of the interaction strength. As shown in Figure 2, there is an obvious competition between both the alkane-alkane and alkane-ZIF interactions, where the average interaction strength between alkanes and ZIF-10 always decreases while that between alkanes themselves increases as the loading increases. By comparison, the predominant one is the increased interaction between alkanes themselves in all cases so that the total interaction strength always increases with the increasing loading, which is unfavorable to the diffusion motions of pure alkanes in ZIF-10 (shown in Figure 1). Furthermore, the absolute values of total interaction energies follow the order  $n\text{-}C_4H_{10} > C_3H_8 > C_2H_6$  at the same loadings, meaning that the total interaction strength of pure alkanes in ZIF-10 gradually increases as the chain length increases. In other words, longer alkanes will suffer more restrictions from ZIF-10, which is consistent with the  $D_i$  order of  $C_2H_6 > C_3H_8 > n\text{-}C_4H_{10}$  in Figure 1.

On the other hand, longer alkanes and higher loadings can also increase the collision frequency among alkanes in ZIF-10. A higher collision frequency can change the velocity directions of alkanes more frequently, which is significantly unfavorable to the diffusion motions. Meanwhile, it should be noted that the alkane collisions in ZIF-10 occur among alkanes themselves and also between alkanes and ZIF-10. In fact, the translational motions of small gas molecules are mainly determined by the relevant interaction energies at the low loadings while those of large gas molecules are dominated by their relevant collision frequency at the high loadings because the interaction energies mainly refer to the long-range attractive interactions while the collision behavior mainly refers to the short-range repulsive interactions. Then, the insight into such microscopic collisions can be gained by the COM velocity autocorrelation functions (VACFs) of alkanes because both kinds of effective collisions can change the magnitude and direction of their velocities, which are favorable to losing the correlation of initial velocities. Therefore, less relaxation time implicitly specifies a higher collision frequency. The normalized VACFs and the relevant relaxation times  $\tau_{\nu}$  can be expressed as 65,66

$$C_{\nu}(t) = \frac{\langle \nu_i(0) \ \nu_i(t) \rangle}{\langle \nu_i(0) \ \nu_i(0) \rangle} \tag{2}$$

and then

$$\tau_{\nu} = \int_{0}^{\infty} C_{\nu}(t) \, \mathrm{d}t \tag{3}$$

where  $v_i(t)$  is the velocity of gas molecule type i at time t. The angular brackets denote the ensemble average. As shown in Figure 3, all VACF curves are found to cross the axis and then become negative. The negative regions in all VACF curves mean that the alkane molecules are moving in the direction opposite to that at t = 0 due to the collision effect, which is the characteristic of rattling motion of alkanes in ZIF-10. Accordingly, the variations of relaxation times as a function of the loading are shown in the insets of Figure 3. A shorter relaxation time means a higher collision frequency for alkanes in ZIF-10, which is unfavorable to the relevant diffusion motions. Therefore, we can find the same loading-dependent behavior between the relaxation time of VACF and the diffusion coefficients  $D_i$ . In this way, we can capture the diffusion behavior qualitatively during a short simulation time, and the VACF is more sensitive and convenient than the MSD in identifying the diffusion motions of longer alkanes in porous media.

Besides the translational motions, the rotational motions are also an important dynamics property of  $C_2H_6$ ,  $C_3H_8$ , and n- $C_4H_{10}$  molecules in ZIF-10, especially for longer alkanes. Herein, the relevant rotational dynamics is studied through the corresponding time correlation function (TCF)  $C_r(t)$ , <sup>67,68</sup>

$$C_r(t) = \left\langle P_l \left( \frac{1}{N} \sum_{i=1}^{N} \mathbf{u}_i(t) \, \mathbf{u}_i(0) \right) \right\rangle \tag{4}$$

where  $P_l$  is the lth rank Legendre polynomial (l = 1 and 2), N is the number of alkanes in ZIF-10, and  $\mathbf{u}_i$  is the unit vector of

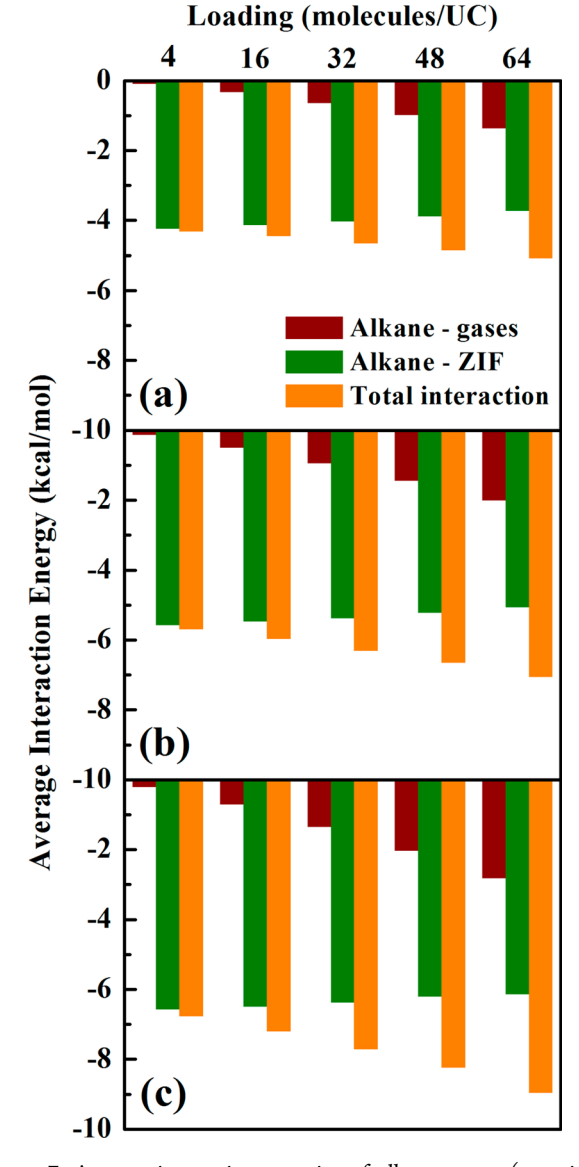


**Figure 7.** Average interaction energies of alkane—gases (containing alkane—alkane and alkane— $CO_2$  interactions) and alkane—ZIF and total interaction energy for (a)  $C_2H_6$ , (b)  $C_3H_8$ , and (c)  $n\text{-}C_4H_{10}$  molecules of their mixtures with  $CO_2$  in ZIF-10 at different loadings. All standard deviations here are less than  $\pm 0.02$  kcal/mol. The error bars are smaller than the symbol size, so they are not shown.

the *i*th alkane at time *t*. The angular brackets mean that the ensemble averaging is taken over the tagged alkanes at different reference initial times. In this work, the orientation of each alkane molecule is represented by a vector pointing from the terminal carbon group to the other terminal carbon group. Figure 4 shows that the rotational  $C_r(t)$  curves (l=2) of the  $n\text{-}C_4H_{10}$  molecules decay more slowly than those of  $C_2H_6$  and  $C_3H_8$  molecules as the loading increases, suggesting that  $n\text{-}C_4H_{10}$  molecules rotate more slowly than both the  $C_2H_6$  and  $C_3H_8$  molecules in ZIF-10. In order to gain the rotational relaxation times  $\tau_r$ , these  $C_r(t)$  curves are fitted by a three-parameter exponential function (with a total weight of 1, i.e., A+B+C=1),  $^{65,68,69}$ 

$$C_{\rm r}(t) = A \exp(-t/\tau_{\rm a}) + B \exp(-t/\tau_{\rm b}) + C \exp(-t/\tau_{\rm c})$$
 (5)

and then

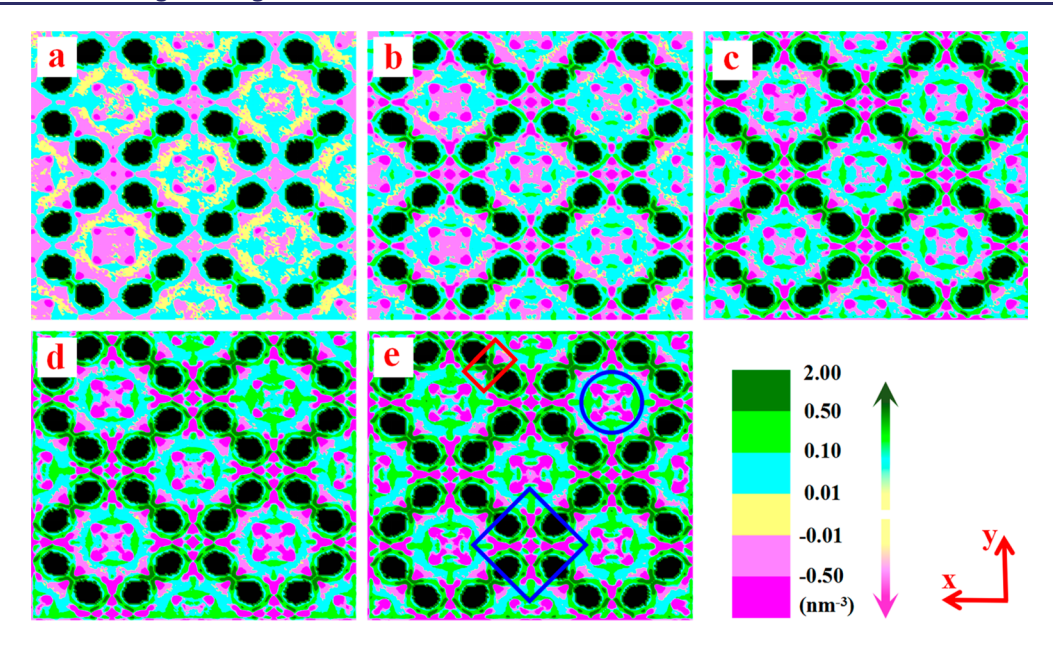


**Figure 8.** Two-dimensional different density distribution in the x-y plane between  $CO_2$  and  $C_2H_6$  in the  $C_2H_6/CO_2$  mixture, where the positive region means that the density of  $CO_2$  molecules is higher than that of  $C_2H_6$  and the negative region means that the density of  $CO_2$  molecules is lower than that of  $C_2H_6$ . The black regions refer to the frameworks without both  $CO_2$  and  $C_2H_6$  molecules. The loadings from 4 to 64 molecules/ UC correspond to a-e.

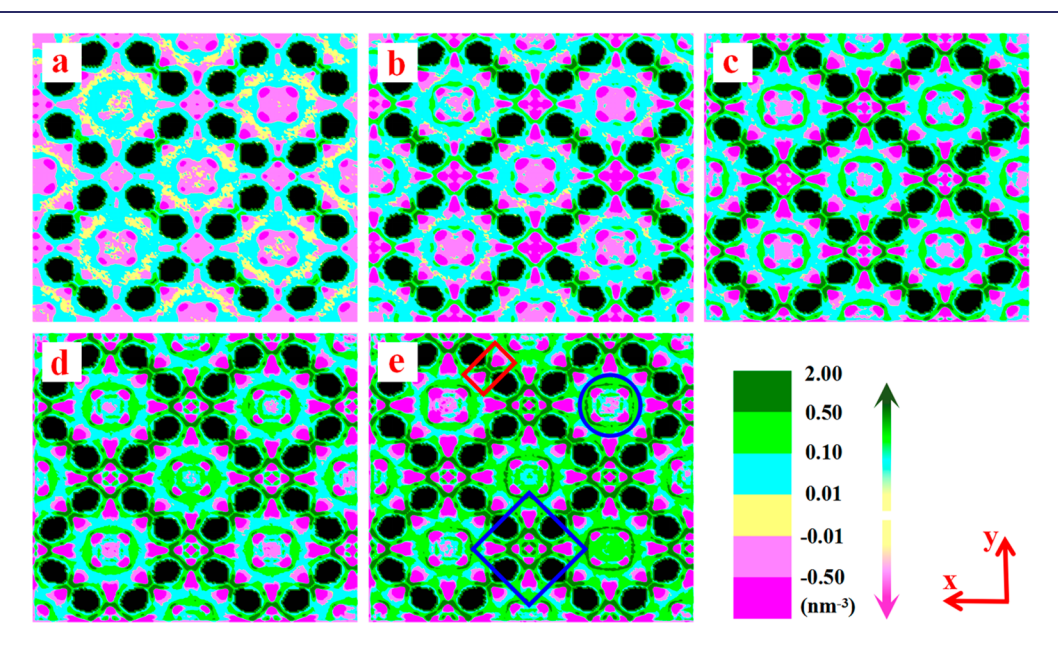
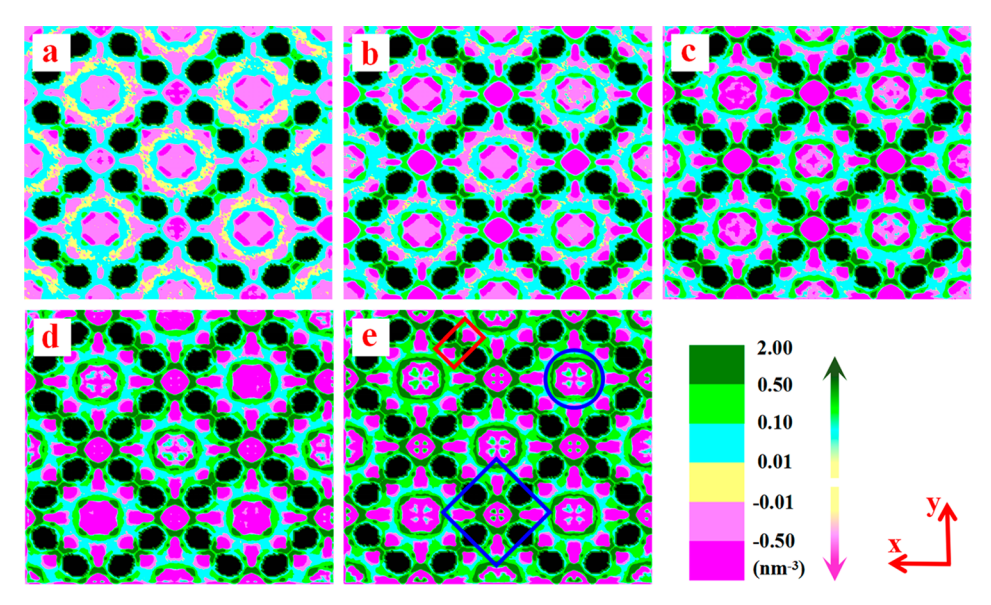


Figure 9. Two-dimensional different density distribution in the x-y plane between  $CO_2$  and  $C_3H_8$  in the  $C_3H_8/CO_2$  mixture, where the positive region means that the density of  $CO_2$  molecules is higher than that of  $C_3H_8$  and the negative region means that the density of  $CO_2$  molecules is lower than that of  $C_3H_8$ . The black regions refer to the frameworks without both  $CO_2$  and  $C_3H_8$  molecules. The loadings from 4 to 64 molecules/ UC correspond to a-e.

$$\tau_{\rm r} = A\tau_{\rm a} + B\tau_{\rm b} + C\tau_{\rm c} \tag{6}$$

where A, B, and C are fitting parameters, while  $\tau_a$ ,  $\tau_b$ , and  $\tau_c$  are the time constants. The calculated  $\tau_r$  values are illustrated in Figure 4d. It can be clearly observed that all  $\tau_r$  values of n-C<sub>4</sub>H<sub>10</sub> molecules in ZIF-10 are always much larger than those of C<sub>2</sub>H<sub>6</sub> and C<sub>3</sub>H<sub>8</sub> molecules at the same loadings. Moreover, the difference between these  $\tau_r$  values among different alkanes is found to become larger and larger as the loading increases. For example, the  $\tau_r$  values are 3.71, 7.56, and 7.91 ps in turn for C<sub>2</sub>H<sub>6</sub>, C<sub>3</sub>H<sub>8</sub>, and n-C<sub>4</sub>H<sub>10</sub> molecules at 4 molecules/UC while the corresponding values are 0.92, 22.05, and 52.82 ps at

64 molecules/UC, respectively. More importantly, the  $\tau_{\rm r}$  values initially show a decrease with the increasing loading and then follow an increase at high loadings, especially for longer  $C_3H_8$  and  $n\text{-}C_4H_{10}$  molecules. Namely, their rotational motions are initially accelerated and then decelerated gradually beyond a critical loading regardless of the chain length, which is very different from the monotonic decrease in the diffusion rate with loading (Figure 1). Such different loading-dependent behavior between the translational and the rotational motions originates mainly from the fact that the translational motion is a kind of global dynamics property while the rotational motion is a kind



**Figure 10.** Two-dimensional different density distribution in the x-y plane between  $CO_2$  and  $n-C_4H_{10}$  in the  $n-C_4H_{10}/CO_2$  mixture, where the positive region means the density of  $CO_2$  molecules is higher than that of  $n-C_4H_{10}$  and the negative region means the density of  $CO_2$  molecules is lower than that of  $n-C_4H_{10}$ . The black regions refer to the frameworks without both  $CO_2$  and  $n-C_4H_{10}$  molecules. The loadings from 4 to 64 molecules/UC correspond to a—e.

of local dynamics property. The translational motions of alkanes refer to the migration among different cages of ZIF-10, i.e., the intercage dynamics. However, the rotational motions can occur in the same cages, i.e., the intracage dynamics, which are much more sensitive to the changes of local environment around the alkanes.

To further capture the changes in the local environment, Figure 5 illustrates the two-dimensional density distributions projected on the x-y plane with different loadings for  $C_2H_6$ , C<sub>3</sub>H<sub>8</sub>, and n-C<sub>4</sub>H<sub>10</sub> molecules in ZIF-10. It can be seen from Figure  $5a_1-c_1$  that the adsorption sites of all alkane molecules are located at the internal surfaces of ZIF-10 when the loading is 4 molecules/UC. Accordingly, the average interaction strength between alkanes and ZIF-10 should be the largest at the adsorption sites compared to those at other loadings, which is well supported by the results in Figure 2. In this case, the rotational motions of alkanes in ZIF-10 would be considerably hindered by strong restrictions at the adsorption sites. As the loading increases, Figure 5a2-c4 shows that the internal surfaces have no space to accommodate more alkanes, and then more and more alkanes enter the free center regions of cages in ZIF-10 where these alkane molecules suffer from fewer restrictions and rotate faster than those at the adsorption sites. Therefore, we can find a decreasing process of the rotational relaxation times  $\tau_r$  with the increasing loading at the beginning for  $C_2H_6$ ,  $C_3H_8$ , and n- $C_4H_{10}$  molecules in ZIF-10. When the loading is beyond a critical value, however, the central regions of cages are gradually occupied by more and more alkane molecules so that no free space exists in ZIF-10, as shown in Figure  $5a_5-c_5$ . Those additional alkanes in ZIF-10 cages result in the enhanced alkane—alkane interactions (Figure 2), leading to more restrictions for the rotational motions of all alkanes. Accordingly, we can observe an increasing process of the  $\tau_r$ value from Figure 4d when the loading is beyond a critical loading regardless of the chain length. By comparison with Figure 4d, additionally, it is worth noting that the corresponding critical loading is found to decrease with the increasing chain length of alkanes. For example, the critical loading for the

 $\rm C_2H_6$  molecule is 48 molecules/UC, while the corresponding loadings for  $\rm C_3H_8$  and  $\it n$ - $\rm C_4H_{10}$  molecules are 32 and 16 molecules/UC, respectively. This is because longer alkanes are larger than shorter ones so that longer alkanes need more free space to rotate. Therefore, they are sensitively subjected to restrictions from the increasing loading.

3.2. Equimolar Alkane/CO<sub>2</sub> Mixtures in ZIF-10. Next, we focus on how the presence of CO2 affects the translational and rotational motions of light alkanes in ZIF-10. For better comparisons, equimolar alkane/CO2 mixtures with the same loadings as pure alkanes in ZIF-10 are considered here. Figure 6 presents the variation in the self-diffusion coefficients D, for alkane/CO<sub>2</sub> mixtures with loading as well as the  $D_{i,mix}/D_{i,pure}$ ratios for alkanes in ZIF-10 to evaluate the effects from the presence of CO<sub>2</sub>. Then, we can see from Figure 6a-c that all  $D_i$  values for  $C_2H_6$ ,  $C_3H_8$ , and n- $C_4H_{10}$  molecules in the presence of CO<sub>2</sub> show a monotonically decreasing trend with loading and are smaller than that of CO<sub>2</sub> molecules, especially for C<sub>3</sub>H<sub>8</sub> and n-C<sub>4</sub>H<sub>10</sub> molecules. As shown in Figure 6d, meanwhile, all ratios of  $D_{i,mix}/D_{i,pure}$  for alkanes are larger than 1 over all studied loadings and increase significantly with the increasing loading, where the  $D_{i,mix}/D_{i,pure}$  value for n-C<sub>4</sub>H<sub>10</sub> molecules in ZIF-10 is even up to around 20 at 64 molecules/ UC. This clearly indicates that the presence of CO<sub>2</sub> molecules can promote the acceleration of the translational motions of alkanes in ZIF-10 for all mixtures and such promotion effects become more and more significant as the loading increases, especially for long n-C<sub>4</sub>H<sub>10</sub>/CO<sub>2</sub> mixtures.

Likewise, Figure 7 shows the average interaction energies of three different alkanes in their mixtures with  $\rm CO_2$  in ZIF-10 at all loadings. In the mixture cases, the total interaction energies of alkanes in ZIF-10 include the alkane—alkane, alkane— $\rm CO_2$ , and alkane—ZIF interaction energies. By comparison, the absolute values of their total interaction energies are found to increase with the increasing loading, which mainly results from the increased alkane—gas interactions (including alkane—alkane and alkane— $\rm CO_2$  interactions) over the decreased alkane—ZIF interactions. The increase in the total interaction

energies with loading leads to the decreased  $D_i$  values of alkanes in ZIF-10. As shown in Figure S2 of the Supporting Information, the absolute values of CO<sub>2</sub>-ZIF interaction energies are larger than those of the corresponding alkane-ZIF interaction energies regardless of the loading and alkane chain length. This is because the oxygen atoms of CO<sub>2</sub> molecules with partially negative charges can form hydrogen bonds (HBs) with electrondeficient C-H groups of the imidazolate ligands in ZIF-10.60,70-73 As shown in Figure S3, the average number of HBs per CO<sub>2</sub> molecule in ZIF-10 is found to be more than 1.5. Therefore, CO2 molecules should preferentially occupy the area around the imidazolate ligands in ZIF-10 compared to alkanes, which can be well supported by the density deviation distributions of alkane/CO2 mixtures in ZIF-10. Similar phenomena have been reported for alkane/CO2 mixtures in other confinements. 32,35,74,75 Experimentally, Gautam et al. 75 found that CO2 molecules can replace C3H8 molecules from the pore walls of nanoporous silica aerogel so that more C<sub>3</sub>H<sub>8</sub> molecules become available and excitable. In other words, the addition of CO<sub>2</sub> molecules can enhance the jump rates of C<sub>3</sub>H<sub>8</sub> molecules and then increase their diffusion coefficient.

Figures 8–10 show the density deviation distributions between alkanes and CO2 molecules in ZIF-10, where the color is green when the density of CO<sub>2</sub> molecules is higher than that of alkanes and magenta otherwise. As illustrated in Figure 8, the interaction sites mainly correspond to the red rectangle and blue diamond regions, which are close to the imidazolate ligands of ZIF-10. As the loading increases, CO<sub>2</sub> molecules are found to accumulate at the four-membered window in the red rectangle due to the strong HB interactions between CO2 molecules and imidazolate rings, while most of the C2H6 molecules are located in the larger space of the MER cage in the blue circle and the intercage region in the blue diamond. Larger available space is favorable to diffusion and rotational motions of C<sub>2</sub>H<sub>6</sub> molecules. As shown in Figures 9 and 10 (i.e., mixtures of  $C_3H_8/CO_2$  and  $n-C_4H_{10}/CO_2$ ),  $CO_2$  is initially distributed at the four-membered window in the red rectangle at 4 molecules/UC and then CO<sub>2</sub> molecules are gradually enriched and take up the interaction sites of  $C_3H_8$  (or n- $C_4H_{10}$ ) in the blue diamond as the loading increases. Especially for the  $n-C_4H_{10}/CO_2$  mixture, n-C<sub>4</sub>H<sub>10</sub> molecules are found be trapped by the surrounding CO<sub>2</sub> molecules, shown by the blue diamond in Figure 10. Also, the additional alkane molecules from the loading increase, generally stay away from the strong interaction sites, and are concentrated in the large center region of the MER cage, as labeled in the blue circled region. When most of the interaction sites of alkanes in ZIF-10 are replaced by CO<sub>2</sub> molecules, weakened interactions between alkanes and ZIF-10 can resulting, a situation that is favorable to the diffusive motions of alkanes. Furthermore, a larger amount of available free space should be able to reduce the collision frequency of alkanes in ZIF-10, promoting both diffusional and rotational motions of alkanes.

Figure 11 presents the relaxation times of VACF curves for alkane molecules in the pure and mixture cases. Accordingly, those detailed VACF curves at different loadings are shown in Figure S4 of the Supporting Information. The comparison results clearly demonstrate that the relaxation times in the mixture case are always larger than those in the pure case, indicating a decrease in the collision frequency of alkanes in ZIF-10 in the presence of CO<sub>2</sub>. In particular, the collision relaxation times for  $n\text{-C}_4\text{H}_{10}/\text{CO}_2$  mixtures are much larger than those for pure  $n\text{-C}_4\text{H}_{10}$  in ZIF-10, meaning that the collision frequency of  $n\text{-C}_4\text{H}_{10}$  in ZIF-10 is considerably reduced in the

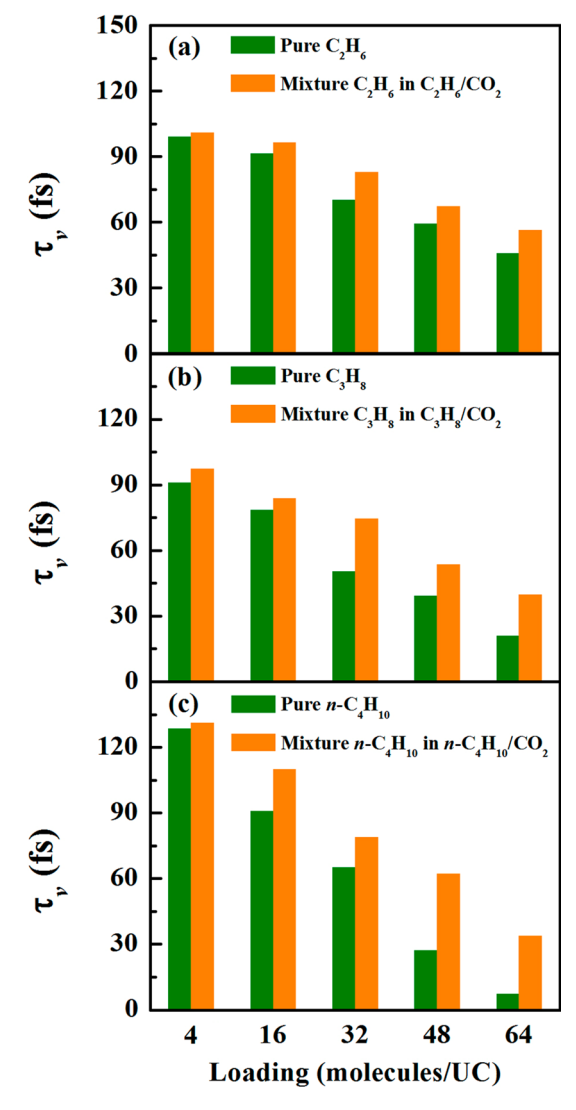


**Figure 11.** Contrast of the relaxation time from VACF curves for alkane molecules in the pure and mixture systems. All standard deviations here are less than  $\pm 2.0$  fs. The error bars are smaller than the symbol size, so they are not shown.

presence of CO2, which is significantly favorable to their diffusion rate. Furthermore, the differences in relaxation time between pure alkanes and alkane/CO2 mixtures in ZIF-10 are gradually increasing as the loading increases. Therefore, the presence of CO<sub>2</sub> molecules can promote the diffusion motion of alkanes in ZIF-10 for all mixtures, and such a promotion effect becomes more and more significant as the loading increases, as shown in Figure 11. Moreover, Figure 12 presents the rotational TCF curves and the corresponding  $\tau_r$  values of alkanes molecules in ZIF-10 in the presence of CO<sub>2</sub>. By comparison with Figure 12a-c, we find that the TCF curves of C<sub>2</sub>H<sub>6</sub>, C<sub>3</sub>H<sub>8</sub>, and n-C<sub>4</sub>H<sub>10</sub> decay much faster in mixture cases than in pure cases. Similarly, Figure 12d shows that the  $\tau_{r,pure}$  $\tau_{\rm r.mix}$  ratio is larger than 1, indicating that the relaxation times of the mixture system are also smaller than those of the pure systems. Therefore, the presence of CO<sub>2</sub> molecules can also promote the rotational motions of alkanes for all studied mixtures due to the decreased collision frequency of alkanes in

To better understand the role of confinement from ZIF-10, we have performed additional MD simulations for pure alkanes

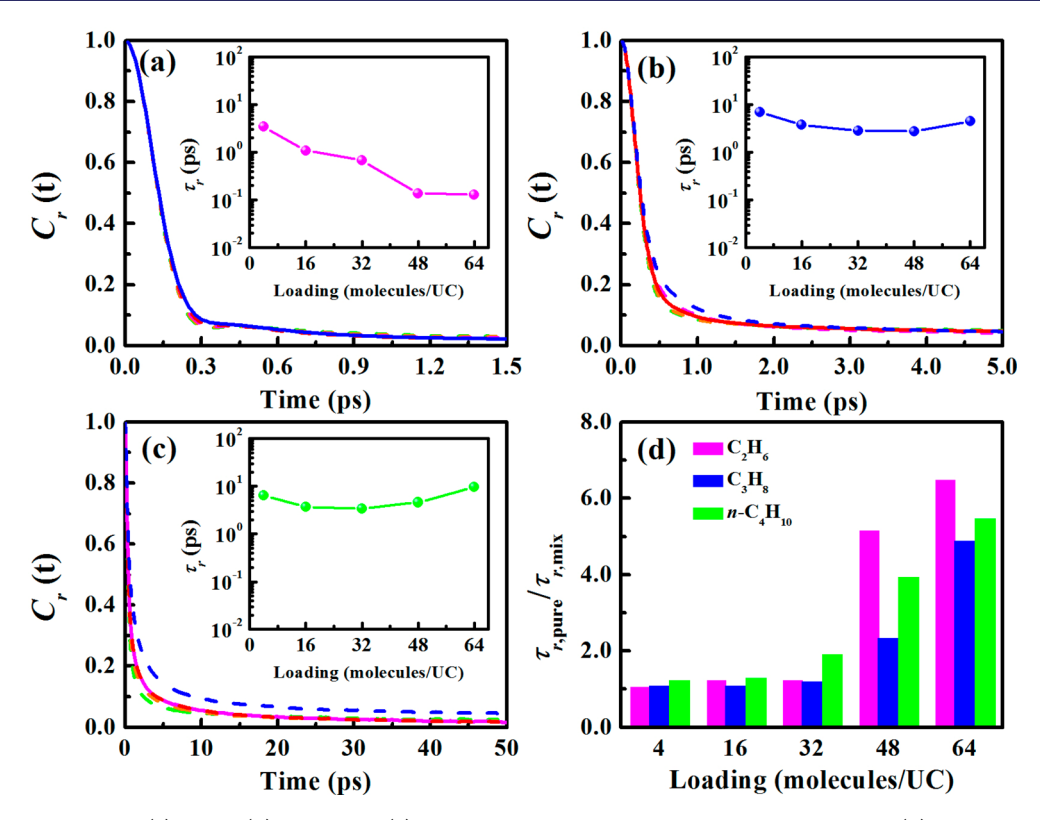


Figure 12. Rotational TCFs of (a)  $C_2H_6$ , (b)  $C_3H_8$ , and (c) n- $C_4H_{10}$  in their mixtures at different loadings and (d) the  $\tau_{r,pure}/\tau_{r,mix}$  ratio. Green, orange, magenta, red, and blue lines correspond to the loadings from 4 to 64 molecules/UC in turn. The relevant values and standard deviations are listed in Table S6 of the Supporting Information.

and equimolar alkane/CO<sub>2</sub> mixtures (including two loadings of 4 and 64 molecules/UC) in the same simulation box only without ZIF-10. Figure 13 presents the calculated  $D_{i,mix}/D_{i,pure}$ and  $\tau_{\rm r,pure}/\tau_{\rm r,mix}$  ratios in the system without ZIF-10. For the loading of 4 molecules/UC, both the  $D_{i,\text{mix}}/D_{i,\text{pure}}$  and  $\tau_{r,\text{pure}}/D_{i,\text{pure}}$  $\tau_{\rm r,mix}$  ratios for these three alkanes are smaller than 1, suggesting that the presence of CO<sub>2</sub> molecules restricts their translational and rotational motions at the lowest loading. On the contrary, the presence of CO2 molecules can accelerate the translational and rotational motions of these three alkanes in ZIF-10, as shown in Figures 6 and 12. For the loading of 64 molecules/UC, the  $D_{i,\text{mix}}/D_{i,\text{pure}}$  and  $\tau_{r,\text{pure}}/\tau_{r,\text{mix}}$  ratios for these three alkanes are found to be a bit more than 1, which is much smaller than the corresponding values of  $D_{i,mix}/D_{i,pure}$ and  $\tau_{\rm r,pure}/\tau_{\rm r,mix}$  in ZIF-10 (Figures 6 and 12). Therefore, the confinement of ZIF-10 can significantly promote the acceleration effect of CO2 molecules on the translational and rotational motions of alkanes.

#### 4. CONCLUSIONS

In this work, the loading-dependent translational and rotational behavior of pure  $C_2H_6$ ,  $C_3H_8$ , and  $n\text{-}C_4H_{10}$  and their binary equimolar mixtures with  $CO_2$  in ZIF-10 has been investigated by a series of classical MD simulations. Our simulation results show that self-diffusion coefficients  $D_i$  for pure alkanes in ZIF-10 decreased monotonically with increased loading partly due to the competition between the enhanced alkane—alkane and the weakened alkane—ZIF interactions, where the unfavorable contribution of the former increase dominates the favorable contribution of the latter decrease. Accordingly, the total interaction strength of all pure alkanes in ZIF-10 is also found to increase as the loading increases. Furthermore, the

corresponding collision frequency of pure alkanes in ZIF-10 obviously increases with loading, which can hinder their translational motions considerably. Nevertheless, the dependence of their rotational motions on the loading is found to be significantly different from that of their translational motions. Their rotational motions are initially accelerated and then decelerated gradually beyond a critical loading regardless of the chain length. Such different loading-dependent behavior between the translational and rotational motions is mainly due to the fact that the translational motion is a global intercage dynamics property relating to the migration among different cages while the rotational motion is a local intracage dynamics property occurring in the same cages. Therefore, the initial acceleration of their rotational motions can be attributed to the fact that more alkane molecules are not adsorbed at the internal surfaces of MER cages but rather are adsorbed into the free center regions of cages in ZIF-10, which can be clearly captured by the relevant two-dimensional density distributions. Furthermore, a loading higher than the corresponding critical value can result in a considerable decrease in free space within the whole ZIF-10 so that more restrictions hinder their rotational motions.

However, our simulation results reveal that the presence of  $\rm CO_2$  molecules can significantly accelerate both the translational and rotational motions for alkanes in ZIF-10 at the same loading partly due to the lower steric resistance of smaller  $\rm CO_2$  molecules compared to that of longer alkane molecules. Especially for  $n\text{-}C_4\text{H}_{10}/\text{CO}_2$  in ZIF-10, the value of  $D_{i,\text{mix}}/D_{i,\text{pure}}$  is up to around 20 at the highest loading of 64 molecules/UC. Meanwhile, the strong hydrogen bonds with the imidazolate rings can cause  $\rm CO_2$  molecules to preferentially occupy the adsorption sites in ZIF-10 compared to alkanes, leading to the

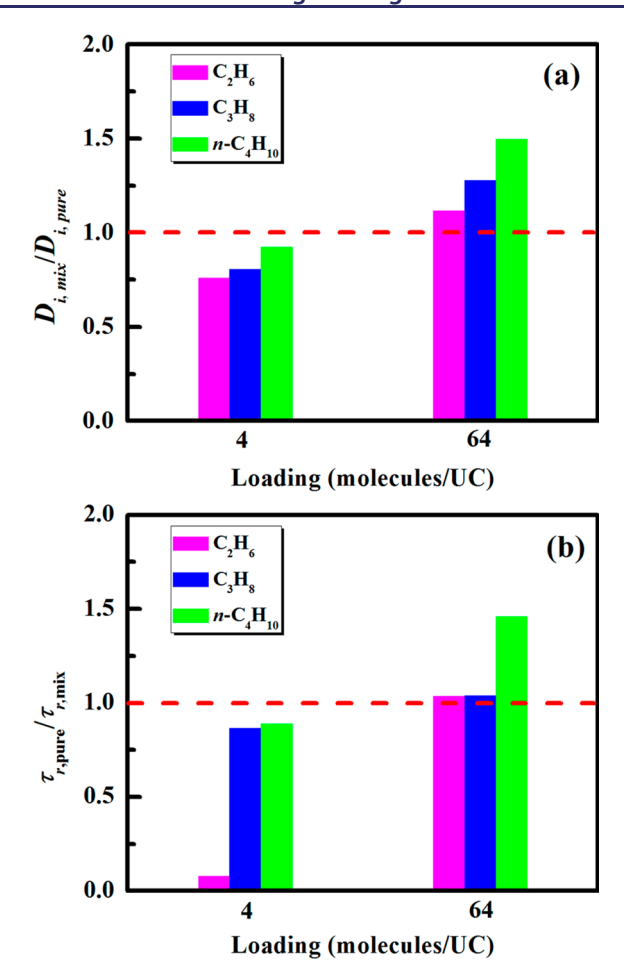


**Figure 13.** (a)  $D_{i,mix}/D_{i,pure}$  and (b)  $\tau_{r,pure}/\tau_{r,mix}$  ratios under loadings of 4 and 64 molecules/UC in the same simulation boxes without ZIF-10.

weakened interactions between alkanes and ZIF-10. Such competitive adsorption behavior can be observed at the molecular level from the density deviation distributions of alkane/CO<sub>2</sub> mixtures in ZIF-10. More importantly, the competitive adsorption between alkanes and CO2 molecules can also significantly reduce the collision frequency for alkanes in ZIF-10, which is quite favorable to both the translational and rotational motions of alkanes in ZIF-10. In addition, the confinement of ZIF-10 is also found to significantly promote the acceleration effect of CO<sub>2</sub> molecules with respect to the translational and rotational motions of alkanes. The simulation results in this work provide a molecular-level understanding of the translational and rotational motions of pure alkanes and alkane/CO2 mixtures in ZIF-10 and are of great benefit to experimental scientists in designing and preparing new ZIFs and their membranes for various gas separations.

# ASSOCIATED CONTENT

#### S Supporting Information

The Supporting Information is available free of charge on the ACS Publications website at DOI: 10.1021/acs.jced.8b00651.

Lennard-Jones parameters and partial atomic charges used in this work; compositions of alkane/CO<sub>2</sub> mixtures in corresponding bulk phases; MSD curves of pure alkane molecules in ZIF-10; interaction energies between gas molecules and ZIF-10 in three mixture systems; average HB number per CO<sub>2</sub> in ZIF-10; VACF curves of binary mixtures in ZIF-10; all rotational

relaxation times in this work; self-diffusion coefficients of alkane molecules without ZIF-10; and self-diffusion coefficients for gas molecules (PDF)

# AUTHOR INFORMATION

#### **Corresponding Authors**

\*E-mail: yangzhen@jxnu.edu.cn (Z.Y.).

\*E-mail: hll@ou.edu (L.H.).

\*E-mail: cxs66cn@jxnu.edu.cn (X.C.).

#### ORCID ®

Zhen Yang: 0000-0002-5205-3281 Liangliang Huang: 0000-0003-2358-9375

#### Note

The authors declare no competing financial interest.

# ACKNOWLEDGMENTS

This work was supported by the National Natural Science Foundation of China (nos. 21306070, 21463011, and 21863005), the Natural Science Foundation of Jiangxi Province (no. 20171BAB203012), the Special Program for Applied Research on Super Computation of the NSFC-Guangdong Joint Fund (the second phase) under grant no. U1501501, and the Sponsored Program for Cultivating Youths of Outstanding Ability in Jiangxi Normal University. L.H. acknowledges the U.S. National Science Foundation for support through grant CHE-1710102.

# REFERENCES

- (1) Zhang, X.; Sun, Y.; Su, W.; Wang, X. Adsorption Equilibria of C1-C4 from Natural Gas on Graphene Sheets. *J. Chem. Eng. Data* **2016**, *61*, 1667–1675.
- (2) Bao, Z.; Alnemrat, S.; Yu, L.; Vasiliev, I.; Ren, Q.; Lu, X.; Deng, S. Adsorption of Ethane, Ethylene, Propane, and Propylene on a Magnesium-Based Metal-Organic Framework. *Langmuir* **2011**, 27, 13554–13562.
- (3) Duan, J.; Higuchi, M.; Foo, M. L.; Horike, S.; Rao, K. P.; Kitagawa, S. A Family of Rare Earth Porous Coordination Polymers with Different Flexibility for  $CO_2/C_2H_4$  and  $CO_2/C_2H_6$  Separation. *Inorg. Chem.* **2013**, *52*, 8244–8249.
- (4) Phan, A.; Cole, D. R.; Weiss, R. G.; Dzubiella, J.; Striolo. A Confined Water Determines Transport Properties of Guest Molecules in Narrow Pores. *ACS Nano* **2016**, *10*, 7646–7656.
- (5) Wang, H.; Cao, D. Diffusion and Separation of  $H_2$ ,  $CH_4$ ,  $CO_2$ , and  $N_2$  in Diamond-Like Frameworks. *J. Phys. Chem. C* **2015**, *119*, 6324–6330.
- (6) Luyben, W. L. Control of an Extractive Distillation System for the Separation of CO<sub>2</sub> and Ethane in Enhanced Oil Recovery Processes. *Ind. Eng. Chem. Res.* **2013**, *52*, 10780–10787.
- (7) Liu, H.; Cooper, V. R.; Dai, S.; Jiang, D. Windowed Carbon Nanotubes for Efficient CO<sub>2</sub> Removal from Natural Gas. *J. Phys. Chem. Lett.* **2012**, *3*, 3343–3347.
- (8) Vrbová, V.; Ciahotný, K. Upgrading Biogas to Biomethane Using Membrane Separation. *Energy Fuels* **2017**, *31*, 9393–9401.
- (9) Chen, Z.; Gong, H.; Bao, Y.; Wu, W. Engineering Operation Performance of Catalytic Deoxygenation Equipment for Landfill Gas Upgrading. *Energy Fuels* **2017**, *31*, 4565–4570.
- (10) Luo, P.; Zhang, Y.; Wang, X.; Huang, S. Propane-Enriched CO<sub>2</sub> Immiscible Flooding For Improved Heavy Oil Recovery. *Energy Fuels* **2012**, *26*, 2124–2135.
- (11) Ahmed, I.; Jhung, S. H. Applications of Metal-Organic Frameworks in Adsorption/Separation Processes via Hydrogen Bonding Interactions. *Chem. Eng. J.* **2017**, *310*, 197–215.
- (12) Pimentel, B. R.; Lively, R. P. Enabling Kinetic Light Hydrocarbon Separation via Crystal Size Engineering of ZIF-8. *Ind. Eng. Chem. Res.* **2016**, *55*, 12467–12476.

- (13) Herm, Z. R.; Bloch, E. D.; Long, J. R. Hydrocarbon Separations in Metal-Organic Frameworks. *Chem. Mater.* **2014**, *26*, 323–338.
- (14) Li, J. R.; Kuppler, R. J.; Zhou, H. C. Selective Gas Adsorption and Separation in Metal—Organic Frameworks. *Chem. Soc. Rev.* **2009**, 38, 1477—1504.
- (15) Colón, Y. J.; Snurr, R. Q. High-Throughput Computational Screening of Metal-Organic Frameworks. *Chem. Soc. Rev.* **2014**, *43*, 5735–5749.
- (16) Wu, H.; Gong, Q.; Olson, D. H.; Li, J. Commensurate Adsorption of Hydrocarbons and Alcohols in Microporous Metal Organic Frameworks. *Chem. Rev.* **2012**, *112*, 836–868.
- (17) Becker, T. M.; Heinen, J.; Dubbeldam, D.; Lin, L. C.; Vlugt, T. J. H. Polarizable Force Fields for CO<sub>2</sub> and CH<sub>4</sub> Adsorption in M-MOF-74. *J. Phys. Chem. C* **2017**, 121, 4659–4673.
- (18) Nijem, N.; Wu, H.; Canepa, P.; Marti, A.; Balkus, K. J., Jr.; Thonhauser, T.; Li, J.; Chabal, Y. J. Tuning the Gate Opening Pressure of Metal—Organic Frameworks (MOFs) for the Selective Separation of Hydrocarbons. *J. Am. Chem. Soc.* **2012**, *134*, 15201—15204
- (19) Erucar, I.; Keskin, S. High CO<sub>2</sub> Selectivity of an Amine-Functionalized Metal Organic Framework in Adsorption-Based and Membrane-Based Gas Separations. *Ind. Eng. Chem. Res.* **2013**, *52*, 3462–3472.
- (20) Zhang, L.; Wu, G.; Jiang, J. Adsorption and Diffusion of CO<sub>2</sub> and CH<sub>4</sub> in Zeolitic Imidazolate Framework-8: Effect of Structural Flexibility. *J. Phys. Chem. C* **2014**, *118*, 8788–8794.
- (21) Rankin, R. B.; Liu, J.; Kulkarni, A. D.; Johnson, J. K. Adsorption and Diffusion of Light Gases in ZIF-68 and ZIF-70: A Simulation Study. *J. Phys. Chem. C* **2009**, *113*, 16906–16914.
- (22) Liu, J.; Keskin, S.; Sholl, D. S.; Johnson, J. K. Molecular Simulations and Theoretical Predictions for Adsorption and Diffusion of CH<sub>4</sub>/H<sub>2</sub> and CO<sub>2</sub>/CH<sub>4</sub> Mixtures in ZIFs. *J. Phys. Chem. C* **2011**, *115*, 12560–12566.
- (23) Krishna, R.; van Baten, J. M. Investigating the Relative Influences of Molecular Dimensions and Binding Energies on Diffusivities of Guest Species Inside Nanoporous Crystalline Materials. J. Phys. Chem. C 2012, 116, 23556–23568.
- (24) Ramsahye, N. A.; Gao, J.; Jobic, H.; Llewellyn, P. L.; Yang, Q.; Wiersum, A. D.; Koza, M. M.; Guillerm, V.; Serre, C.; Zhong, C. L.; Maurin, G. Adsorption and Diffusion of Light Hydrocarbons in UiO-66(Zr): A Combination of Experimental and Modeling Tools. *J. Phys. Chem. C* 2014, *118*, 27470–27482.
- (25) Rezlerová, E.; Zukal, A.; Cejka, J.; Siperstein, F. R.; Brennan, J. K.; Lísal, M. Adsorption and Diffusion of C1 to C4 Alkanes in Dual-Porosity Zeolites by Molecular Simulations. *Langmuir* **2017**, 33, 11126–11137.
- (26) Ford, D. C.; Dubbeldam, D.; Snurr, R. Q.; Künzel, V.; Wehring, M.; Stallmach, F.; Kärger, J.; Müller, U. Self-Diffusion of Chain Molecules in the Metal—Organic Framework IRMOF-1: Simulation and Experiment. *J. Phys. Chem. Lett.* **2012**, *3*, 930—933.
- (27) Déroche, I.; Maurin, G.; Borah, B. J.; Yashonath, S.; Jobic, H. Diffusion of Pure  $CH_4$  and Its Binary Mixture with  $CO_2$  in Faujasite NaY: A Combination of Neutron Scattering Experiments and Molecular Dynamics Simulations. J. Phys. Chem. C **2010**, 114, 5027–5034.
- (28) Salles, F.; Jobic, H.; Devic, T.; Guillerm, V.; Serre, C.; Koza, M. M.; Ferey, G.; Maurin, G. Diffusion of Binary CO<sub>2</sub>/CH<sub>4</sub> Mixtures in the MIL-47(V) and MIL-53(Cr) Metal—Organic Framework Type Solids: A Combination of Neutron Scattering Measurements and Molecular Dynamics Simulations. *J. Phys. Chem. C* **2013**, *117*, 11275—11284.
- (29) Hähnel, T.; Kalies, G.; Krishna, R.; Moellmer, J.; Hofmann, J.; Kobalz, M.; Krautscheid, H. Adsorptive Separation of C2/C3/C4-hydrocarbons on a Flexible Cu-MOF: The Influence of Temperature, Chain Length and Bonding Character. *Microporous Mesoporous Mater.* **2016**, 224, 392–399.
- (30) Jobic, H.; Rosenbach, N., Jr.; Ghoufi, A.; Kolokolov, D. I.; Yot, P. G.; Devic, T.; Serre, C.; Ferey, G.; Maurin, G. Unusual Chain-Length Dependence of the Diffusion of *n*-Alkanes in the Metal-

- Organic Framework MIL-47(V): the Blowgun Effect. *Chem. Eur. J.* **2010**, *16*, 10337–10341.
- (31) Li, J.; Li, S.; Zheng, A.; Liu, X.; Yu, N.; Deng, F. Solid-state NMR Studies of Host—Guest Interaction between UiO-67 and Light Alkane at Room Temperature. *J. Phys. Chem. C* **2017**, *121*, 14261—14268.
- (32) Patankar, S.; Gautam, S.; Rother, G.; Podlesnyak, A.; Ehlers, G.; Liu, T.; Cole, D. R.; Tomasko, D. L. Role of Confinement on Adsorption and Dynamics of Ethane and an Ethane—CO<sub>2</sub> Mixture in Mesoporous CPG Silica. *J. Phys. Chem. C* **2016**, *120*, 4843–4853.
- (33) Luo, Y.; Funke, H. H.; Falconer, J. L.; Noble, R. D. Adsorption of CO<sub>2</sub>, CH<sub>4</sub>, C<sub>3</sub>H<sub>8</sub>, and H<sub>2</sub>O in SSZ-13, SAPO-34, and T-Type Zeolites. *Ind. Eng. Chem. Res.* **2016**, *55*, 9749–9757.
- (34) Borah, B.; Zhang, H.; Snurr, R. Q. Diffusion of Methane and Other Alkanes in Metal-Organic Frameworks for Natural Gas Storage. *Chem. Eng. Sci.* **2015**, *124*, 135–143.
- (35) Le, T.; Striolo, A.; Cole, D. R.  $CO_2-C_4H_{10}$  Mixtures Simulated in Silica Slit Pores: Relation between Structure and Dynamics. *J. Phys. Chem. C* **2015**, *119*, 15274–15284.
- (36) Tan, J. C.; Bennett, T. D.; Cheetham, A. K. Chemical Structure, Network Topology, and Porosity Effects on the Mechanical Properties of Zeolitic Imidazolate Frameworks. *Proc. Natl. Acad. Sci. U. S. A.* **2010**, *107*, 9938–9943.
- (37) Wang, B.; Côté, A. P.; Furukawa, H.; O'Keeffe, M.; Yaghi, O. M. Colossal Cages in Zeolitic Imidazolate Frameworks as Selective Carbon Dioxide Reservoirs. *Nature* **2008**, *453*, 207–211.
- (38) Furukawa, H.; Ko, N.; Go, Y. B.; Aratani, N.; Choi, S. B.; Choi, E.; Yazaydin, A. O.; Snurr, R. Q.; O'Keeffe, M.; Kim, J.; Yaghi, O. M. Ultrahigh Porosity in Metal-Organic Frameworks. *Science* **2010**, 329, 424–428.
- (39) Ding, L.; Yazaydin, A. O. The Effect of SO<sub>2</sub> on CO<sub>2</sub> Capture in Zeolitic Imidazolate Frameworks. *Phys. Chem. Chem. Phys.* **2013**, *15*, 11856–11861.
- (40) Wu, Y.; Chen, H.; Liu, D.; Qian, Y.; Xi, H. Adsorption and Separation of Ethane/Ethylene on ZIFs with Various Topologies: Combining GCMC Simulation with the Ideal Adsorbed Solution Theory (IAST). *Chem. Eng. Sci.* **2015**, *124*, 144–153.
- (41) Krokidas, P.; Castier, M.; Moncho, S.; Brothers, E.; Economou, I. G. Molecular Simulation Studies of the Diffusion of Methane, Ethane, Propane, and Propylene in ZIF-8. *J. Phys. Chem. C* **2015**, *119*, 27028–27037.
- (42) Eum, K.; Jayachandrababu, K. C.; Rashidi, F.; Zhang, K.; Leisen, J.; Graham, S.; Lively, R. P.; Chance, R. R.; Sholl, D. S.; Jones, C. W.; Nair, S. Highly Tunable Molecular Sieving and Adsorption Properties of Mixed-Linker Zeolitic Imidazolate Frameworks. *J. Am. Chem. Soc.* **2015**, *137*, 4191–4197.
- (43) Gücüyener, C.; van den Bergh, J.; Gascon, J.; Kapteijn, F. Ethane/Ethene Separation Turned on Its Head: Selective Ethane Adsorption on the Metal-Organic Framework ZIF-7 through a Gate-Opening Mechanism. J. Am. Chem. Soc. 2010, 132, 17704–17706.
- (44) Keskin, S. Atomistic Simulations for Adsorption, Diffusion, and Separation of Gas Mixtures in Zeolite Imidazolate Frameworks. *J. Phys. Chem. C* **2011**, *115*, 800–807.
- (45) Verploegh, R. J.; Nair, S.; Sholl, D. S. Temperature and Loading-Dependent Diffusion of Light Hydrocarbons in ZIF-8 as Predicted Through Fully Flexible Molecular Simulations. *J. Am. Chem. Soc.* **2015**, *137*, 15760–15771.
- (46) Witherspoon, V. J.; Yu, L. M.; Jawahery, S.; Braun, E.; Moosavi, S. M.; Schnell, S. K.; Smit, B.; Reimer, J. A. Translational and Rotational Motion of C8 Aromatics Adsorbed in Isotropic Porous Media (MOF-5): NMR Studies and MD Simulations. *J. Phys. Chem. C* 2017, 121, 15456–15462.
- (47) Rosenbach, N., Jr.; Jobic, H.; Ghoufi, A.; Devic, T.; Koza, M. M.; Ramsahye, N.; Mota, C. J.; Serre, C.; Maurin, G. Diffusion of Light Hydrocarbons in the Flexible MIL-53(Cr) Metal—Organic Framework: A Combination of Quasi-Elastic Neutron Scattering Experiments and Molecular Dynamics Simulations. *J. Phys. Chem. C* **2014**, *118*, 14471–14477.

- (48) Kolokolov, D. I.; Jobic, H.; Rives, S.; Yot, P. G.; Ollivier, J.; Trens, P.; Stepanov, A. G.; Maurin, G. Diffusion of Benzene in the Breathing Metal—Organic Framework MIL-53(Cr): A Joint Experimental—Computational Investigation. *J. Phys. Chem. C* **2015**, *119*, 8217—8225.
- (49) Allen, F. H. The Cambridge Structural Database: a Quarter of a Million Crystal Structures and Rising. *Acta Crystallogr., Sect. B: Struct. Sci.* **2002**, *58*, 380–388.
- (50) Zheng, C.; Liu, D.; Yang, Q.; Zhong, C.; Mi, J. Computational Study on the Influences of Framework Charges on CO<sub>2</sub> Uptake in Metal–Organic Frameworks. *Ind. Eng. Chem. Res.* **2009**, *48*, 10479–10484.
- (51) Chokbunpiam, T.; Fritzsche, S.; Caro, J.; Chmelik, C.; Janke, W.; Hannongbua, S. Importance of ZIF-90 Lattice Flexibility on Diffusion, Permeation, and Lattice Structure for an adsorbed  $\rm H_2/CH_4$  Gas Mixture: A Re-Examination by Gibbs Ensemble Monte Carlo and Molecular Dynamics Simulations. *J. Phys. Chem. C* **2017**, *121*, 10455–10462.
- (52) Chokbunpiam, T.; Fritzsche, S.; Parasuk, V.; Caro, J.; Assabumrungrat, S. Molecular simulations of a CO<sub>2</sub>/CO mixture in MIL-127. *Chem. Phys. Lett.* **2018**, *696*, 86–91.
- (53) Saha, D.; Bao, Z. B.; Jia, F.; Deng, S. G. Adsorption of CO<sub>2</sub>, CH<sub>4</sub>, N<sub>2</sub>O, and N<sub>2</sub> on MOF-5, MOF-177, and Zeolite 5A. *Environ. Sci. Technol.* **2010**, 44, 1820–1826.
- (54) Bakker, W. J. W.; Kapteijn, F.; Poppe, J.; Moulijn, J. A. Permeation Characteristics of a Metal-Supported Silicalite-1 Zeolite Membrane. *J. Membr. Sci.* **1996**, *117*, 57–78.
- (55) Martin, M. G.; Siepmann, J. I. Transferable Potentials for Phase Equilibria. 1. United-Atom Description of *n*-Alkanes. *J. Phys. Chem. B* **1998**, *102*, 2569–2577.
- (56) Potoff, J. J.; Siepmann, J. I. Vapor-liquid Equilibria of Mixtures Containing Alkanes, Carbon Dioxide, and Nitrogen. *AIChE J.* **2001**, 47. 1676–1682.
- (57) Siepmann, J. I.; Frenkel, D. Configurational bias Monte Carlo: A New Sampling Scheme for Flexible Chains. *Mol. Phys.* **1992**, *75*, 59–70
- (58) Yeh, I. C.; Hummer, G. System-Size Dependence of Diffusion Coefficients and Viscosities from Molecular Dynamics Simulations with Periodic Boundary Conditions. J. Phys. Chem. B 2004, 108, 15873—15870
- (59) Heyes, D. M.; Cass, M. J.; Powles, J. G.; Evans, W. A. B. Self-Diffusion Coefficient of the Hard-Sphere Fluid: System Size Dependence and Empirical Correlations. *J. Phys. Chem. B* **2007**, 111, 1455–1464.
- (60) Li, L.; Yang, D.; Fisher, T. R.; Qiao, Q.; Yang, Z.; Hu, N.; Chen, X.; Huang, L. Molecular Dynamics Simulations for Loading-Dependent Diffusion of CO<sub>2</sub>, SO<sub>2</sub>, CH<sub>4</sub>, and Their Binary Mixtures in ZIF-10: The Role of Hydrogen Bond. *Langmuir* **2017**, *33*, 11543–11553.
- (61) Hockney, R. W.; Eastwood, J. W. Computer Simulation Using Particles, 2nd ed.; IOP: Bristol, U.K., 1988.
- (62) Plimpton, S. Fast Parallel Algorithms for Short-Range Molecular Dynamics. J. Comput. Phys. 1995, 117, 1–19.
- (63) Leach, A. R. Molecular Modelling: Principles and Applications, 2nd ed.; Prentice-Hall: London, 2001.
- (64) Li, Y.; Yang, Z.; Hu, N.; Zhou, R.; Chen, X. Insights into Hydrogen Bond Dynamics at the Interface of the Charged Monolayer-Protected Au Nanoparticle from Molecular Dynamics Simulation. *J. Chem. Phys.* **2013**, *138*, 184703.
- (65) Yang, Z.; Li, Y.; Zhou, G.; Chen, X.; Tao, D.; Hu, N. Molecular Dynamics Simulations of Hydrogen Bond Dynamics and Far-Infrared Spectra of Hydration Water Molecules around the Mixed Monolayer-Protected Au Nanoparticle. *J. Phys. Chem. C* **2015**, *119*, 1768–1781.
- (66) Martí, J.; Padro, J. A.; Guàrdia, E. Molecular Dynamics Simulation of Liquid Water along the Coexistence Curve: Hydrogen Bonds and Vibrational Spectra. J. Chem. Phys. 1996, 105, 639.
- (67) Laage, D.; Hynes, J. T. A Molecular Jump Mechanism of Water Reorientation. *Science* **2006**, *311*, 832–835.

- (68) Fu, F.; Li, Y.; Yang, Z.; Zhou, G.; Huang, Y.; Wan, Z.; Chen, X.; Hu, N.; Li, W.; Huang, L. Molecular-Level Insights into Size-Dependent Stabilization Mechanism of Gold Nanoparticles in 1-Butyl-3-methylimidazolium Tetrafluoroborate Ionic Liquid. *J. Phys. Chem. C* 2017, 121, 523–532.
- (69) Sinha, S. K.; Chakraborty, S.; Bandyopadhyay, S. Thickness of the Hydration Layer of a Protein from Molecular Dynamics Simulation. *J. Phys. Chem. B* **2008**, *112*, 8203–8209.
- (70) Horton, H. R.; Moran, L. A.; Ochs, R. S.; Rawn, J. D.; Scrimgeour, K. G. *Principles of Biochemistry*, 3rd ed.; Prentice Hall: Upper Saddle River, NJ, 1996.
- (71) Liu, J.; Thallapally, P. K.; McGrail, B. P.; Brown, D. R.; Liu, J. Progress in Adsorption-Based CO<sub>2</sub> Capture by Metal-Organic Frameworks. *Chem. Soc. Rev.* **2012**, *41*, 2308–2322.
- (72) Boulmene, R.; Boussouf, K.; Prakash, M.; Komiha, N.; Al-Mogren, M. M.; Hochlaf, M. Ab Initio and DFT Studies on  $CO_2$  Interacting with  $Zn^{q+}$ -Imidazole (q=0,1,2) Complexes: Prediction of Charge Transfer through  $\sigma$  or  $\pi$ -Type Models. *ChemPhysChem* **2016**, 17, 994–1005.
- (73) Lau, G. P. S.; Schreier, M.; Vasilyev, D.; Scopelliti, R.; Grätzel, M.; Dyson, P. J. New Insights into the Role of Imidazolium-Based Promoters for the Electroreduction of CO<sub>2</sub> on a Silver Electrode. *J. Am. Chem. Soc.* **2016**, *138*, 7820–7823.
- (74) Wu, H.; Chen, J.; Liu, H. Molecular Dynamics Simulations about Adsorption and Displacement of Methane in Carbon Nanochannels. *J. Phys. Chem. C* **2015**, *119*, 13652–13657.
- (75) Gautam, S.; Liu, T.; Rother, G.; Jalaivo, N.; Marmontov, E.; Welch, S.; Sheets, J.; Droege, M.; Cole, D. R. Dynamics of Propane in Nanoporous Silica Aerogel: A Quasi-Elastic Neutron Scattering Study. *J. Phys. Chem. C* **2015**, *119*, 18188–18195.